Modelling of patterned fibre constrained layer damping for composite materials

André P. Verstappen
Department of Mechanical Engineering, University of Canterbury, Christchurch, New Zealand.
John R. Pearse
Department of Mechanical Engineering, University of Canterbury, Christchurch, New Zealand.

Summary
Vibration damping is an important consideration in the design of fibre reinforced composite structures as these stiff, lightweight materials often have undesirable vibration transmission characteristics. If not properly addressed, high vibration levels can propagate throughout a structure and result in undesirable conditions for occupants and equipment. It is possible to incorporate viscoelastic damping layers into a composite laminate's construction to achieve improved damping properties. Inclusion of embedded viscoelastic layers results in a constrained layer damping configuration, where the damping capacity is governed by the shear strain in the damping layer. Deliberate asymmetry in orthotropic layers surrounding a viscoelastic core can be used to induce coupling between normal and shear effects. A finite element model is presented to investigate the effect of patterned fibre constraining layers on the damping performance of these constrained layer materials.

PACS no. 43.40.+s, 46.40.Ff, 02.70.Dh

1. Introduction

The use of composite materials is becoming increasingly prevalent in a wide range of industries. Many of the application areas for such materials are in structures and environments where high levels of vibration are also present.

A method of increasing the damping characteristics of composite constructions is through inclusion of viscoelastic damping layers within a laminate lay-up. The damping performance of these constructions is influenced by the shear strains within the viscoelastic layers in the same way as constrained layer damping (CLD) surface treatments. Use of asymmetric orthotropic layers surrounding a viscoelastic core produces coupling between extension and twist behaviours. This coupling can be used to induce in-plane transverse shear strains. Previous research into the use of 'zig-zag' and continuous sinusoidal fibre patterns in such a configuration found that the damping performance of these composite damping materials was affected by the fibre pattern wavelength and maximum fibre angle [1-4]. The pattern wavelength tended to shift the frequency at which maximum damping occurred, while the maximum fibre angle shifted the maximum damping value achieved. Previous research considered simple constant sine wave patterns. An example is shown in Figure 1.

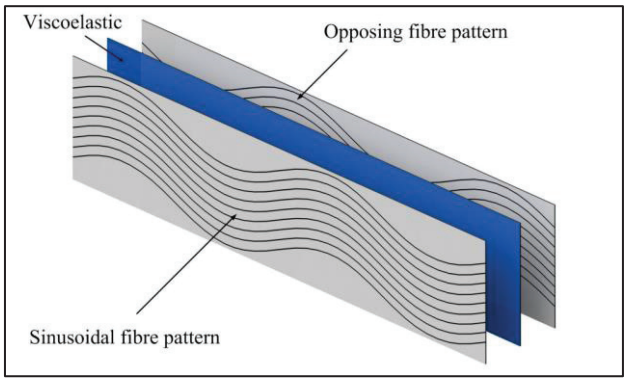

Figure 1. Simple sinusoidal fibre pattern.

It is of interest to explore what effect more complex fibre patterns have on the damping spectrum of composite sandwich arrangements with a viscoelastic core material. An example of a more complex pattern is shown in Figure 2.

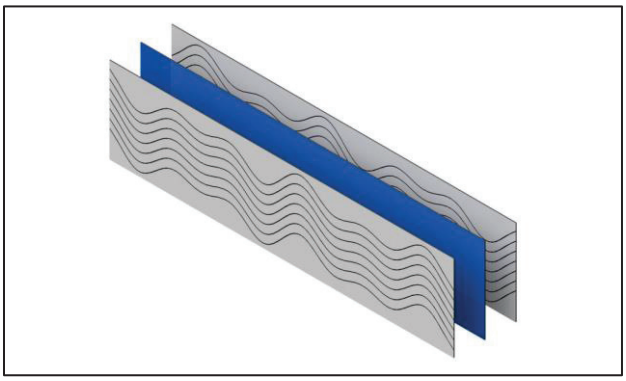

Figure 2. Complex sinusoidal fibre pattern.

The proposed composite damping treatment, termed complex patterned fibre constrained layer damping (CPF-CLD), presents fabrication challenges which prohibit economic production of large volumes of test specimens. Hence, finite element analysis (FEA) is an excellent technique for an investigation of this composite damping material.

This paper presents the development of a finite element model (FEM) in MATLAB to investigate the modal damping behaviour of three-layer CPF-CLD beams.

2. Key Considerations

The CPF-CLD material varies from conventional composite laminate constructions in several significant areas:

- Structural properties vary along the length of the sample depending on the local fibre angle,
- In-plane transverse shear strains are present due to the fibre angle phase shift between layers,
- The mid ply is viscoelastic with damping and stiffness properties that vary significantly with excitation frequency,
- The fibre-reinforced polymer (FRP) face sheets provide some material damping to the system and will also exhibit frequency dependent material properties.

Element types, material models and other analysis parameters must be correctly selected in order to properly reflect these characteristics in the model.

3. Element Type

Solid elements were selected for the model to account for transverse in-plane shear effects. In order to prevent shear locking, quadratic interpolation functions were used in the plane of the laminate and linear interpolation functions through the thickness. This configuration was achieved using 16-node brick elements. The 'brick-16' arrangement is shown in Figure 3.

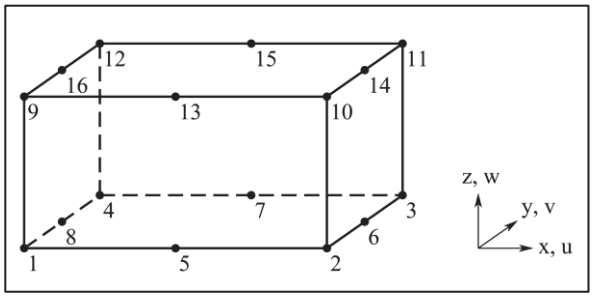

Figure 3. 'Brick-16' solid element.

Three of these 'Brick-16' elements were stacked to represent the three layers present in the laminate construction. This produced a layered brick with 32 nodes, shown in Figure 4.

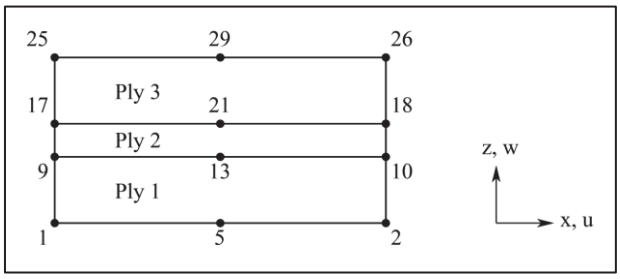

Figure 4. Stacked 'Brick-16' solid elements.

Isoparametric element formulation was used to facilitate the solid elements taking non-rectangular shapes due to deformation. This was achieved by transforming a deformed 'brick-16' element into a coordinate system where the element became a cube. The new element coordinate system was defined by directions ξ, η, and ζ which mapped to the global coordinate system directions x, y, and z respectively. Element edge lengths in the element coordinate system were all set to 2, with the origin located at the centre of each element. Thus, nodes were located at values of -1, 0, +1 in the ξ and η directions, and at -1 and +1 in the ζ direction.

Quadratic interpolation functions were used in the laminate plane, and linear interpolation functions

were used in the thickness direction. This resulted in a 16 x 1 interpolation function vector of the form:

$$\begin{Bmatrix} N_1 \\ N_2 \\ N_3 \\ N_4 \\ N_5 \\ N_6 \\ N_7 \\ N_8 \\ N_9 \\ N_{10} \\ N_{11} \\ N_{12} \\ N_{13} \\ N_{14} \\ N_{15} \\ N_{16} \end{Bmatrix} = \frac{1}{8} \begin{Bmatrix} (1-\xi)(1-\eta)(-\xi-\eta-1)(1-\zeta) \\ (1+\xi)(1-\eta)(\xi-\eta-1)(1-\zeta) \\ (1+\xi)(1+\eta)(\xi+\eta-1)(1-\zeta) \\ (1-\xi)(1+\eta)(-\xi+\eta-1)(1-\zeta) \\ 2(1-\xi^2)(1-\eta)(1-\zeta) \\ 2(1+\xi)(1-\eta^2)(1-\zeta) \\ 2(1-\xi^2)(1+\eta)(1-\zeta) \\ 2(1-\xi)(1-\eta^2)(1-\zeta) \\ (1-\xi)(1-\eta)(-\xi-\eta-1)(1+\zeta) \\ (1+\xi)(1-\eta)(\xi-\eta-1)(1+\zeta) \\ (1+\xi)(1+\eta)(\xi+\eta-1)(1+\zeta) \\ (1-\xi)(1+\eta)(-\xi+\eta-1)(1+\zeta) \\ 2(1-\xi^2)(1-\eta)(1+\zeta) \\ 2(1+\xi)(1-\eta^2)(1+\zeta) \\ 2(1-\xi^2)(1+\eta)(1+\zeta) \\ 2(1-\xi)(1-\eta^2)(1+\zeta) \end{Bmatrix}. \quad (1)$$

Each node had three translational degrees of freedom. Interpolation functions were applied to each degree of freedom resulting in a 3 x 48 interpolation function matrix of the form:

$$[N] = \begin{bmatrix} N_1 \dots N_{16} & 0 \dots 0 & 0 \dots 0 \\ 0 \dots 0 & N_1 \dots N_{16} & 0 \dots 0 \\ 0 \dots 0 & 0 \dots 0 & N_1 \dots N_{16} \end{bmatrix}. \quad (2)$$

The displacements within each 'brick-16' element could then be defined by:

$$\begin{Bmatrix} u \\ v \\ w \end{Bmatrix} = \begin{Bmatrix} \sum N_i u_i \\ \sum N_i v_i \\ \sum N_i w_i \end{Bmatrix} = [N]\{a\}, \quad (3)$$

where nodal displacements were defined as:

$$\{a\} = \{u_1 \dots u_{16} \quad v_1 \dots v_{16} \quad w_1 \dots w_{16}\}^T. \quad (4)$$

Transformation between the element coordinate system and the global coordinate system was achieved using the Jacobian matrix [J]. This matrix was used to map the physical lengths ∂x, ∂y and ∂z to the reference lengths $\partial \xi$, $\partial \eta$ and $\partial \zeta$. The Jacobian matrix was of the form:

$$[J] = \begin{bmatrix} \sum N_{i,\xi} x_i & \sum N_{i,\xi} y & \sum N_{i,\xi} z_i \\ \sum N_{i,\eta} x_i & \sum N_{i,\eta} x_i & \sum N_{i,\eta} x_i \\ \sum N_{i,\zeta} x_i & \sum N_{i,\zeta} x_i & \sum N_{i,\zeta} x_i \end{bmatrix}, \quad (5)$$

where comma separated subscripts indicate partial derivatives in that dimension.

The element stiffness matrix, $[k^*]$, was defined by:

$$[k^*] = \iiint_{-1}^{1} [B]^T [E^*][B]\ J\ d\xi\ d\eta\ d\zeta\ , \quad (6)$$

where $[B]$ was the element strain matrix, $[E^*]$ was the complex material constitutive matrix, and J was the determinant of the Jacobian matrix. The 6 x 48 element strain matrix was defined as:

$$[B] = \begin{bmatrix} N_{1,x} \dots N_{16,x} & \mathbf{0} & \mathbf{0} \\ \mathbf{0} & N_{1,y} \dots N_{16,y} & \mathbf{0} \\ \mathbf{0} & \mathbf{0} & N_{1,z} \dots N_{16,z} \\ \mathbf{0} & N_{1,z} \dots N_{16,z} & N_{1,y} \dots N_{16,y} \\ N_{1,z} \dots N_{16,z} & \mathbf{0} & N_{1,x} \dots N_{16,x} \\ N_{1,y} \dots N_{16,y} & N_{1,x} \dots N_{16,x} & \mathbf{0} \end{bmatrix}. \quad (7)$$

The material constitutive matrix $[E^*]$ was dependent on the material properties of the element under consideration and the orientation of the material within the element. The constitutive matrix was also complex due to the complex stiffness values used to account for the damping within the model. Material property transformations were applied to $[E^*]$ for the outer two plies in order to account for the varying fibre orientation along the length of the structure studied.

The element mass matrix, $[m]$, was defined by:

$$[m] = \iiint_{-1}^{1} \rho [N]^T [N]\ J\ d\xi\ d\eta\ d\zeta\ , \quad (8)$$

where ρ was the density of the material within the element. As the element mass matrix was calculated using the same interpolation functions as used in the computation of the element stiffness matrix, the mass matrix was classed as 'consistent'.

An explicit element damping matrix was not required as the damping behaviour was incorporated by the imaginary terms of $[k^*]$.

The integration required to evaluate $[k^*]$ and $[m]$ was performed using Gauss Quadrature [5, 6]. As quadratic interpolation functions were used in the laminate plane and linear functions in the thickness direction, three Gauss points were used in the ξ

and η directions, and two Gauss points in the ζ direction.

4. Material Models

Calculation of the element stiffness matrices required the use of appropriate material models for the constituent materials. The fibre layers were modelled as a transversely isotropic material while the damping layer was assumed to be isotropic.
The damping properties for both of these material types were accounted for using complex constitutive matrices $[E^*]$. The complexity of the stiffness matrices was a result of complex material properties within the constitutive equations for each of the materials. Many of these properties were also frequency dependent and models for the frequency dependent behaviour were required in order to produce a useful finite element model.

In equation 6, the complex 6 x 6 material constitutive matrix $[E^*]$ was used to derive the 48 x 48 stiffness matrix $[k^*]$ for each 'brick-16' element. For the isotropic viscoelastic damping material (VEM), the material constitutive matrix was defined using the shear modulus version of Hooke's Law for an isotropic material in three dimensions. Damping was accounted for using complex shear modulus:

$$G^*_{VEM} = G_{VEM}(1 + i\eta_{VEM}) \,, \tag{9}$$

where, G_{VEM} is the storage modulus of the VEM when acting in shear, and η_{VEM} is the damping loss factor. Both of these properties were functions of frequency.

The element stiffness matrices for the fibre layers were calculated using the general orthotropic material constitutive equations with the 2-3 (y-z) plane as a plane of symmetry. Transformation of the material constitutive matrix was required as the fibre orientation within each element was dependent upon where the element lay along the fibre pattern. The resulting complex compliance matrix was of the form:

$$[S^*]_{FRP} = \begin{bmatrix} \frac{1}{E_1^*} & \frac{-\nu_{12}}{E_1^*} & \frac{-\nu_{12}}{E_1^*} & & & \\ \frac{-\nu_{12}}{E_1^*} & \frac{1}{E_2^*} & \frac{-\nu_{23}}{E_2^*} & & \mathbf{0} & \\ \frac{-\nu_{12}}{E_1^*} & \frac{-\nu_{23}}{E_2^*} & \frac{1}{E_2^*} & & & \\ & & & \frac{1}{G_{23}^*} & 0 & 0 \\ & \mathbf{0} & & 0 & \frac{1}{G_{12}^*} & 0 \\ & & & 0 & 0 & \frac{1}{G_{12}^*} \end{bmatrix}, \tag{10}$$

where,

$$E_i^* = E_i(1 + i\eta_i) \,, \tag{11}$$

$$G_{ij}^* = G_{ij}\big(1 + i\eta_{ij}\big). \tag{12}$$

The material constitutive matrix could then be defined by:

$$[Q^*]_{FRP} = [S^*]_{FRP}^{-1} \,. \tag{13}$$

The extensional storage moduli (E_1 and E_2) and their associated loss factors (η_1 and η_2), along with the shear storage moduli (G_{12} and G_{23}) and their associated loss factors (η_{12} and η_{23}), were functions of frequency. As with the frequency dependent properties of the VEM, the frequency dependence of these FRP properties were measured using dynamic experiments and added to the finite element model.

A transformation of the FRP material constitutive matrix was performed to account for the local fibre angle within each element. This produced the required constitutive equation, $[E^*]$, for calculation of the element stiffness matrix:

$$[E^*]_{FRP} = [T]^T [Q^*]_{FRP} [T], \tag{14}$$

where the transformation matrix $[T]$ was defined, using $m = \cos(\theta)$ and $n = \sin(\theta)$, as:

$$[T] = \begin{bmatrix} m^2 & n^2 & 0 & 0 & 0 & -mn \\ n^2 & m^2 & 0 & 0 & 0 & -mn \\ 0 & 0 & 1 & 0 & 0 & 0 \\ 0 & 0 & 0 & m & n & m \\ 0 & 0 & 0 & -n & m & 0 \\ 2mn & -2mn & 0 & 0 & 0 & m^2 - n^2 \end{bmatrix}. \tag{15}$$

5. Iterative Damping Analysis

The modal damping performance and deformation behaviour of the model was desired. As the constituent materials properties within the model were functions of frequency, an iterative method was required to solve the model behaviour for each mode of interest. The equation of motion of the modelled system was:

$$[M]\{\ddot{a}\} + [K^*]\{a\} = \{f(t)\}. \quad (16)$$

The forcing vector, displacement vector and acceleration vector could be expressed in the frequency domain using a Laplace transformation and the general solution $s = i\omega$. This resulted in:

$$([K^*] - \omega^2[M])\{A\}e^{i\omega t} = \{F\}e^{i\omega t}\,. \quad (17)$$

In the case of unforced (modal) vibration, equation 17 simplified to:

$$([K^*] - \omega^2[M])\{A\} = \{0\}. \quad (18)$$

Alternatively, equation 18 could be displayed as the general linear eigenproblem, with complex eigenvectors and eigenvalues resulting from the complex stiffness matrix:

$$[K^*][\Phi^*] = [M][\Phi^*][\Lambda^*], \quad (19)$$

where $[\Phi^*]$ is a matrix of the n eigenvectors, $\{\varphi^*\}$, of the system and $[\Lambda^*]$ is a diagonal matrix of the n eigenvalues, λ^*, of the system, where n is the total degrees of freedom of the system.

Solution of this eigenproblem with the MATLAB function *eigs* yielded the first p eigenvectors and eigenvalues of the system:

$$[\Phi^*, \Lambda^*] = eigs([K^*], [M], p, 0). \quad (20)$$

The Iterative Complex Eigensolution (ICE) algorithm [7] was used to calculate the modal frequencies and associated damping loss factors. The modal frequency and damping loss factor of mode r were defined by:

$$\omega_r = \sqrt{\mathrm{Re}(\lambda_r^*)}, \quad (21)$$

$$\eta_r = \frac{\mathrm{Im}(\lambda_r^*)}{\mathrm{Re}(\lambda_r^*)}\,. \quad (22)$$

The iterative process used to determine the loss factor of each mode of interest is shown in Figure 5. The convergence criteria Δ_{max} was set as 0.01%.

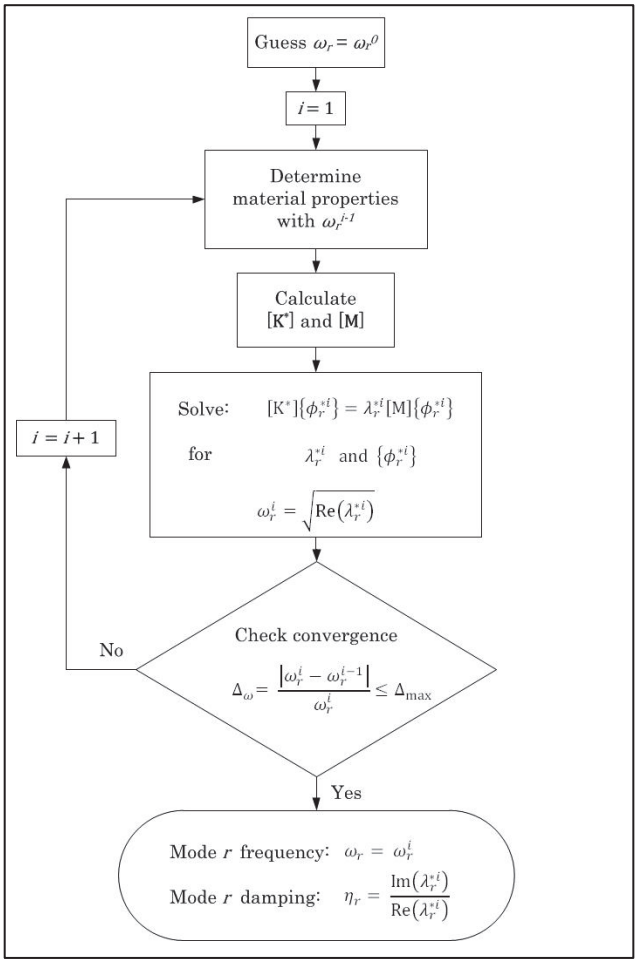

Figure 5. Iterative algorithm to determine modal damping.

6. Fibre Pattern Comparison

Four fibre patterns were compared to the modal damping behaviour produced by unidirectional fibres at 0° orientation. Two fibre pattern types were selected, superposition of two sine waves ($\lambda_1 + \lambda_2$), and swept sine waves ($\lambda_1 \rightarrow \lambda_2$), where λ designated the fibre wavelengths used in the pattern. The specifications of the patterns are shown in Table I.

Table I. Fibre pattern details.

	Pattern 1	Pattern 2	Pattern 3	Pattern 4
Waveform	$\lambda_1 + \lambda_2$	$\lambda_1 + \lambda_2$	$\lambda_1 \rightarrow \lambda_2$	$\lambda_1 \rightarrow \lambda_2$
λ_1 (mm)	125	125	125	125
λ_2 (mm)	50	75	50	75
θ_{max} (°)	30	30	30	30

Figure 6 shows the modal damping performance of the four fibre patterns and the unidirectional layup (UD0) for the first four bending modes of a freely suspended beam.

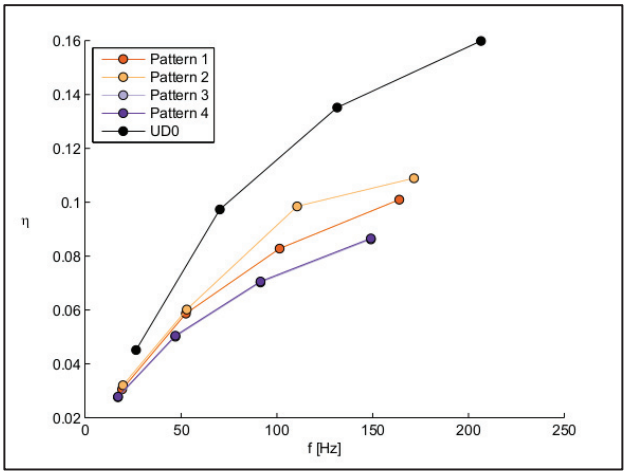

Figure 6. Damping comparison of the first four bending modes.

The results produced by Pattern 3 are obscured by those produced by pattern 4. The trend observed from these results indicated that patterns with lower absolute mean fibre angle (the mean directional stiffness of the pattern) produced increased damping performance. In the case of beams, this indicated that the additional transverse shear strains produced by the patterned fibre layers reduced the stiffness in the length direction of the beam with a net result in reduced modal frequencies and damping values.

Test specimens for the four fibre patterns were fabricated and tested using the materials and methods detailed in [8]. The modal damping results produced by the finite element model typically fell within one standard deviation of the measured experimental values.

7. Further Analyses

The displacement fields defined by the eigenvectors could be used to visualise the strain fields present within the modelled structures. As the eigenvectors only provided relative motion, the strain fields were normalised by the largest strain value to obtain a clearer image of the strain behaviour. Figure 7 shows the shear strains present within the viscoelastic core for the first bending mode of a freely suspended beam using Pattern 2 outer plies.

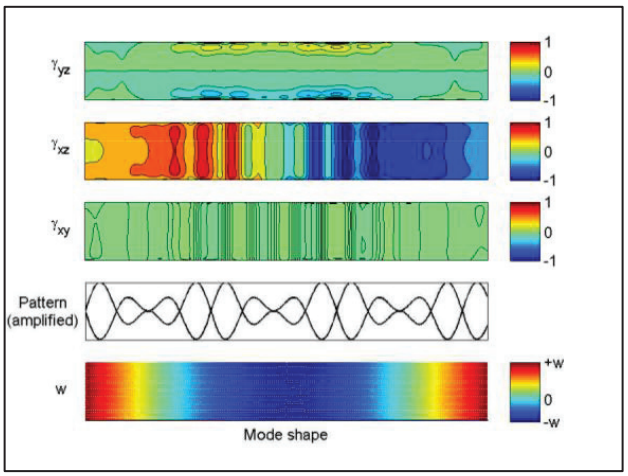

Figure 7. Shear strains within the VEM for Pattern 2 in bending mode 1.

8. Conclusions

The model presented in this paper is capable of modelling the modal damping performance of three layer planar composite materials with a viscoelastic core layer surrounded by patterned fibre layers. The frequency dependence of material properties are accounted for and an iterative solution method is used to ensure the correct material properties are used for each mode of interest.

References

[1] D.D. Olcott: Improved damping in composite structures through stress coupling, co-cured damping layers, and segmented stiffness layers. PhD thesis, Brigham Young University, 1992.

[2] A. Trego, P.F. Eastman: Flexural damping predictions of mechanical elements designed using stress coupled, co-cured damped fiber reinforced composites. Journal of Advanced Materials, 1999. **31**: p. 7-17.

[3] W.F. Pratt, M.S. Allen, C.G. Jensen: Designing with wavy composites. Proc. International SAMPE Symposium and Exhibition 2001.

[4] W.F. Pratt, M.S. Allen, T.J. Skousen: Highly damped lightweight wavy composite. Technical report, Air Force Research Laboratory, 2001.

[5] O.C. Zienkiewicz, R.L. Taylor: The Finite Element Method. Butterworth-Heinemann, Oxford, 2000.

[6] R.D. Cook et al.: Concepts and Applications of Finite Element Analysis. John Wiley & Sons, New York, 2002.

[7] C.M.A. Vasques, R.A.S Moreira, J.D. Rodrigues: Viscoelastic damping technologies – part 1: Modelling and finite element implementation. Journal of Advanced Research in Mechanical Engineering, 2010.

[8] A.P. Verstappen, J.R. Pearse: Patterned fibre constrained layer damping for composite materials. Proc. Internoise 2014.